Edge effects in propagation of terahertz radiation in subwavelength periodic structures

© B. Gelmont¶, R. Parthasarathy, T. Globus

Department of Electrical & Computer Engineering, University of Virginia,
Charlottesville, VA 22904

Improving detection sensitivity of biological molecules with low absorption characteristics in the terahertz gap still remains an important issue in terahertz vibrational resonance spectroscopy. One possible way to increase coupling of incident terahertz radiation to molecules is to exploit local enhancement of electromagnetic field in periodic slot arrays. In this work, we show that periodic arrays of rectangular slots with subwavelength width provide for local electromagnetic field enhancements due to edge effects in our low frequency range of interest, $10-25\,cm^{-1}$. Periodic structures of Au, doped Si and InSb were studied. The half power enhancement width is $\sim 500\,nm$ and less around the slot edges in all cases, thereby possibly bringing terahertz sensing to the nanoscale. InSb is confirmed to offer the highest results with the local power enhancements of the order of 1100 at frequency $14\,cm^{-1}$. InSb and Si have large skin depths in our frequency range of interest and so the analysis of their structures was done through the Fourier expansion method of field diffracted from gratings. Surface impedance boundary conditions were employed to model the Au structure. The applications possibly include development of novel biosensors, and monitoring biophysical processes such as DNA denaturation.

PACS: 41.20.Jb, 78.68.+m, 78.70.Gq,

1. Introduction

The terahertz region (THz) of the electromagnetic spectrum, wedged between the infrared and microwave end, has recently seen a surge in the applications front in areas not limited to imaging, spectroscopy, submillimeter wave astronomy, non-destructive testing, airport security and remote sensing. Vibrational resonance spectroscopy in the THz or sub-THz gap, a reliable technique for fingerprinting species of biological molecules [1–3], has a potential future in broad areas such as biomedicine and biodetection. The absorption spectra of biological molecules in the $0.1-10$ THz range reflect low frequency internal molecular vibrations (weakest hydrogen bonds) and/or non-bonded interactions between different functional groups within molecules. The resonant frequencies of vibrational modes, i.e. phonon modes, serve as specific signatures of species. The low THz end of the spectrum is particularly of interest since water absorption is considerably less than in the far-infrared (far-IR) and infrared (IR) region. However the low absorption characteristics of biological molecules in this region pose the challenge of increasing detection sensitivity of molecules. In order for this to be achieved (and thereby increased reliability), coupling of incident THz radiation to biological molecules has to be enhanced.

An external way to achieve increased coupling of incident radiation is to exploit the local electromagnetic field enhancement provided by subwavelength periodic slot arrays. Slot arrays were used in the THz region as bandpass filters made of lossy metal films and deposited on dielectric membranes [4]. Metallic rough surfaces and periodic structures [5–11] have constantly been of interest experimentally at optical and near-infrared frequencies. It has been recently

demonstrated that waveguide resonance and diffraction are the predominant reasons [8] for enhanced transmission of narrow slot subwavelength (depending on TE or TM polarization, radiation sees a different effective medium) gratings. Extraordinary optical transmission (transmission efficiency exceeding unity when normalized to the surface of the holes) through subwavelength hole arrays was first experimentally observed in Ag [9,10] and attributed to the resonant tunneling of surface plasmons through thin films [10–15]. The THz range also saw studies in this regard recently. Hole arrays in films made of metals (Ag-coated stainless steel [16], Al-coated Si wafers [17]) and doped semiconductors (Si [18] and InSb [19]) were employed. The qualitative analysis of observed transmission enhancement in lossy metallic foils with hole arrays relied on the dispersion of surface plasmons [20] in an uniform film is inappropriate in the case of hole arrays. Hence, the observed enhanced transmission is not well understood. It is to be noted that the transmission properties of subwavelength slot arrays are fundamentally different from arrays of holes, since unlike hole arrays, a slot array can support a propagating mode [21]. Studies on metallic slots were recently done in the THz [22] using the perfect conductor approximation.

We have endeavored to study the mechanism of coupling of TM polarized THz radiation to both metallic and semiconductor films consisting of rectangular slot arrays. In this region, interaction between radiation and metals is quite different from higher frequency regions due to the change in material dielectric properties. The real part of permittivity continues to be negative and is large, but the dissipative imaginary part becomes larger, and hence metals are very conducting and absorbing. Therefore, to reduce radiation losses, it is preferable to substitute metals with doped semiconductors with plasma frequencies in the low
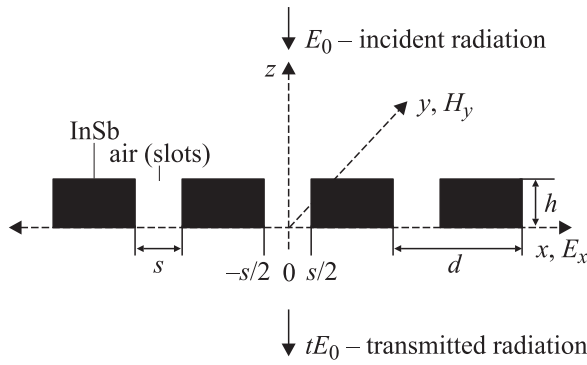

¶ E-mail: gb7k@cms.mail.virginia.edu

Figure 1. The periodic rectangular slot array structure. The axes and the structure parameters (d — spacing, s — slot width, h — film thickness) are shown.

THz range, in order to mimic metallic behavior at high frequencies. InSb, with high electron mobility and low effective mass, is most suited for this purpose. InSb and Si still have a substantial absorbing imaginary part compared to the real component. The absorbing component requires the assumption of a small film thickness, which makes the semiconductor skin depth at both semiconductor–air interfaces larger than half the film thickness throughout our frequency range of interest. This renders the surface impedance boundary conditions [23,24] for perfect conductors to be unsuitable for our case. On the other hand, in contrast with the behavior of metals in short wavelength ranges, the Fourier expansion method for field diffracted from gratings [5] can be applied in the THz region for InSb and Si films, since the imaginary permittivity component damps the Gibbs oscillations [25]. The Fourier expansion method is unsuitable in the THz for Au owing to its dielectric properties. However, since the skin depth in Au is small compared to thickness, surface impedance boundary conditions can be used. Even in this case, thickness is assumed to be very small compared to the wavelength since we employ the perfectly conducting walls approximation [26] for fields inside slots as seen later.

We demonstrate that even in the absence of surface plasmon resonances, increased transmission and local electric field enhancement for TM incidence can be obtained through careful choice of materials and design of periodic slot array structures. We also show that the enhancement of the THz electromagnetic field extends across the slots and reaches peak values at the edges because of discontinuity effects.

2. Theory

We consider a subwavelength array of slots with the periodicity in the x-direction and extending all the way in the y-direction. The z-direction is normal to the plane of incidence. Since the structure is not altered in the y-direction, it would suffice to analyze a two-dimensional

periodic structure as shown in Fig. 1 with the periodicity (spacing) denoted by d, the slot width by s, and the thickness of the film by h. We also consider normal TM incidence (magnetic field parallel to the slot grooves and p-polarized). The relative permittivity in the modulated medium ($0 < z < h$) can be expressed as $e_\parallel(x)$ and the fields inside as H_y^m and E_x^m.

2.1. Fourier expansion method

Inside the modulated medium ($0 < z < h$), the propagation equation [5] is

$$\frac{\partial}{\partial x}\left(\frac{1}{e_\parallel(x)}\frac{\partial H_y^m}{\partial x}\right) + \frac{\partial}{\partial z}\left(\frac{1}{e_\parallel(x)}\frac{\partial H_y^m}{\partial z}\right) + \left(\frac{\omega}{c}\right)^2 H_y^m = 0. \tag{1}$$

Let

$$\tilde{E} = \frac{1}{e_\parallel(x)}\left(\frac{c}{\omega}\right)^2\frac{\partial H_y^m}{\partial z}, \tag{2}$$

again from Maxwell's equations,

$$\nabla \times H^m = -j\omega\left[e_\parallel(x)\varepsilon_0\right]E^m, \tag{3}$$

and so

$$\tilde{E} = \frac{E_x^m}{j\omega\mu_0} = \frac{c^2\varepsilon_0}{j\omega}E_x^m. \tag{4}$$

Substituting Eq. (4) in Eqs (1) and (2) and rearranging,

$$\frac{\partial H_y^m}{\partial z} = \left(\frac{\omega\varepsilon_0}{j}\right)e_\parallel(x)E_x^m, \tag{5}$$

$$\left(\frac{c^2\varepsilon_0}{j\omega}\right)\frac{\partial E_x^m}{\partial z} = -\left(\frac{c}{\omega}\right)^2\frac{\partial}{\partial x}\left(\frac{1}{e_\parallel(x)}\frac{\partial H_y^m}{\partial z}\right) - H_y^m. \tag{6}$$

Eqs. (5) and (6) constitute a coupled differential equation system [5]. Now expanding $e_\parallel(x)$ as a Fourier series with $(N+1)$ modes

$$e_\parallel = \sum_{n=0}^{N} e_n\cos(ngx), \tag{7}$$

where $g = 2\pi/d$.

Projecting the coefficients of the pseudo-periodic electric and magnetic field functions, again on the $\cos(ngx)$ basis, and substituting in Eqs. (5) and (6) for the fields inside the modulated medium, we obtain

$$V_{n,p}\kappa_p = -j\varepsilon_0\omega\sum_{m=0}^{N}(e_\parallel)_{n-m}W_{m,p}, \tag{8}$$

$$W_{n,p}\kappa_p = \left(\frac{j}{\varepsilon_0\omega}\right)ng\sum_{m=0}^{N}mg\left(\frac{1}{e_\parallel}\right)_{n-m}V_{m,p} - V_{n,p}. \tag{9}$$

Coupled set of Eqs. (8) and (9) constitute an eigenvalue problem, which has $2(N+1)$ solutions; κ_p represents the eigenvalues i. e. propagation constants, and $V_{n,p}$, $W_{n,p}$ are the eigenvectors i. e. coefficients associated with the magnetic

and electric fields respectively. The total electric and magnetic fields were expressed as linear combinations of eigenmodes

$$H_y^m = \sum_{p=1}^{2(N+1)} e^{\kappa_p z} A_p \left[\sum_{n=0}^{N} V_{n,p} \cos(ngx) \right], \quad (10)$$

$$E_x^m = \sum_{p=1}^{2(N+1)} e^{\kappa_p z} A_p \left[\sum_{n=0}^{N} W_{n,p} \cos(ngx) \right]. \quad (11)$$

The electric field (E_x^t) in the transmitted medium $(z < 0)$ was written as

$$E_x^t = tE_0 \exp\left(-j \frac{\omega}{c} z \right) + \sum_{n=1}^{N} E_n^t \cos(ngx) \exp(\eta_n z), \quad (12)$$

where $\eta_n = \sqrt{(ng)^2 - (\omega/c)^2}$, E_0 is the amplitude of the incoming wave, E_n is the complex mode amplitude of order n, and t is the transmission coefficient. In the medium of incidence $(z > h)$, the electric field (E_x^i) was written as a superposition of forward and reflected components,

$$E_x^i = E_0 \left(e^{-j(\omega/c)(z-h)} + r e^{j(\omega/c)(z-h)} \right)$$
$$+ \sum_{n=1}^{N} E_n^i \cos(ngx) e^{\eta_n(h-z)}, \quad (13)$$

where r is the reflection coefficient. The magnetic fields were obtained from the electric fields through Maxwell's equations. At the two interfaces, Maxwell's boundary conditions, i.e. continuity of H_y and E_x, were applied to constitute a linear system of equations that can be solved for the unknown field amplitudes in all the regions as well as t and r. Furthermore, the field amplitudes were substituted back into the respective equations to find the electric field enhancements at desired regions relative to the incidence.

2.2. Surface impedance boundary conditions method

The assumption in this method is that the height is very small compared to the spacing and the wavelength. Since the vertical region of radiation interaction is small compared to the horizontal region, the vertical walls of the cavities are assumed to be perfectly conducting while surface impedance boundary conditions are employed at the horizontal surfaces.

The perfectly conducting wall assumption [26] allows us to write the equation for the magnetic field inside the slot cavities $(-s/2 < x < s/2$ and $0 < z < h)$ as

$$H_y^m = \sum_{m=0}^{\infty} \cos\left[\frac{m\pi}{s} \left(x + \frac{s}{2} \right) \right] (A_m e^{-i\beta_m z} + B_m e^{i\beta_m z}), \quad (14)$$

where $\beta_m = \sqrt{(\omega/c)^2 - (m\pi/s)^2}$ and A_m, B_m are the m-mode amplitudes.

In the medium of incidence $(z > h)$, the normalized magnetic field (H_y^i) can be expressed as

$$H_y^i = \sum_{n=-\infty}^{\infty} \left[\delta_{n,0} e^{-i(\omega/c)(z-h)} + \rho_n e^{i\eta_n(z-h)} \right] e^{ingx}. \quad (15)$$

Here ρ_n is the amplitude of n-th reflected order (reflection coefficient $r = \rho_0$). In the transmitted medium, the normalized magnetic field (H_y^t) is

$$H_y^t = \sum_{n=-\infty}^{\infty} \tau_n e^{-i\eta_n z} e^{ingx}, \quad (16)$$

τ_n is the amplitude of the n-th transmitted order, far-field transmission coefficient $t = \tau_0$. The normalized electric fields $(E_x^i$ and $E_x^t)$ can be obtained from the corresponding magnetic fields.

Boundary condition for the magnetic fields at $z = h$ implies

$$\sum_{n=-\infty}^{\infty} (\delta_{n,0} + \rho_n) e^{ingx} = \sum_{m=0}^{\infty} \cos\left[\frac{m\pi}{s} \left(x + \frac{s}{2} \right) \right]$$
$$\times (A_m e^{-i\beta_m h} + B_m e^{i\beta_m h}). \quad (17)$$

Continuity of $(\partial H_y / \partial z)$ $(z = h)$ leads to

$$\sum_{n=-\infty}^{\infty} \left[\delta_{n,0} \left(\frac{\omega}{c} \right) - \rho_n \eta_n \right] e^{ingx} = \sum_{m=0}^{\infty} \cos\left[\frac{m\pi}{s} \left(x + \frac{s}{2} \right) \right]$$
$$\times \beta_m (A_m e^{-i\beta_m h} - B_m e^{i\beta_m h}). \quad (18)$$

At $z = 0$, the corresponding boundary conditions are

$$\sum_{n=-\infty}^{\infty} \tau_n e^{ingx} = \sum_{m=0}^{\infty} \cos\left[\frac{m\pi}{s} \left(x + \frac{s}{2} \right) \right] (A_m + B_m), \quad (19)$$

$$\sum_{n=-\infty}^{\infty} \tau_n \eta_n e^{ingx} = \sum_{m=0}^{\infty} \cos\left[\frac{m\pi}{s} \left(x + \frac{s}{2} \right) \right] \beta_m (A_m - B_m). \quad (20)$$

The other set of conditions utilize the concept of a nonzero tangential component of electric field at the metal surface, and are known as surface impedance boundary conditions.

At $z = h$,

$$\sum_{n=-\infty}^{\infty} \left[\delta_{n,0} \left(\frac{\omega}{c} \right) - \rho_n \eta_n \right] e^{ingx}$$
$$= \left(\frac{\omega}{c} \right) Z_s \sum_{n=-\infty}^{\infty} (\delta_{n,0} + \rho_n) e^{ingx}, \quad (21)$$

where $Z_s = 1/\sqrt{\varepsilon_m}$, ε_m is the relative permittivity of metal.

At $z = 0$,

$$\sum_{n=-\infty}^{\infty} \tau_n \eta_n e^{ingx} = -\left(\frac{\omega}{c}\right) Z_s \sum_{n=-\infty}^{\infty} \tau_n e^{ingx}. \qquad (22)$$

Integrating (17) and (19) and projecting over cosine vectors in the interval $(-s/2, s/2)$

$$\sum_{n=-\infty}^{\infty} I_{n,m}^+ (\delta_{n,0} + \rho_n) = \left(\frac{1+\delta_{m,0}}{2}\right)(A_m e^{-i\beta_m h} + B_m e^{i\beta_m h}), \qquad (23)$$

$$\sum_{n=-\infty}^{\infty} I_{n,m}^+ \tau_n = \left(\frac{1+\delta_{m,0}}{2}\right)(A_m + B_m), \qquad (24)$$

$$I_{n,m}^{\pm} = \frac{1}{s} \int_{-s/2}^{s/2} \cos\left[\frac{m\pi}{s}\left(x + \frac{s}{2}\right)\right] e^{\pm ingx} dx. \qquad (25)$$

Integrating (18) and (21) over limits of validity after projecting over exponential vectors,

$$\left[\delta_{m,0}\left(\frac{\omega}{c}\right) - \rho_m \eta_m\right] = \sum_{n=0}^{\infty} \tilde{I}_{m,n}^- \beta_n (A_n e^{-i\beta_n h} - B_n e^{i\beta_n h})$$

$$+ \left(\frac{\omega}{c}\right) Z_s \frac{1}{d} \sum_{n=-\infty}^{\infty}\left[\int_{-d/2}^{d/2}(\delta_{n,0} + \rho_n) e^{ingx} e^{-imgx} dx\right.$$

$$\left. - \int_{-s/2}^{s/2}(\delta_{n,0} + \rho_n) e^{ingx} e^{-imgx} dx\right], \qquad (26)$$

where

$$\tilde{I}_{m,n} = (s/d) I_{m,n}. \qquad (27)$$

We obtain from boundary condition (17),

$$\left[\delta_{m,0}\left(\frac{\omega}{c}\right) - \rho_m \eta_m\right] = \sum_{n=0}^{\infty} \tilde{I}_{m,n}^- \beta_n (A_n e^{-i\beta_n h} - B_n e^{i\beta_n h})$$

$$+ \left(\frac{\omega}{c}\right) Z_s (\delta_{m,0} - \rho_m \eta_m) - \left(\frac{\omega}{c}\right) Z_s \frac{1}{d}$$

$$\times \sum_{n=0}^{\infty} \int_{-s/2}^{s/2} \cos\left[\frac{n\pi}{s}\left(x + \frac{s}{2}\right)\right](A_n e^{-i\beta_n h} + B_n e^{i\beta_n h}) e^{-imgx} dx. \qquad (28)$$

Using (27) it is possible to rewrite (28) as follows

$$\delta_{m,0}\left[\left(\frac{\omega}{c}\right) - Z_s\left(\frac{\omega}{c}\right)\right] - \rho_m\left[\eta_m + Z_s\left(\frac{\omega}{c}\right)\right] = \sum_{n=0}^{\infty}\left\{\tilde{I}_{m,n}^-\right.$$

$$\left. \times \left(A_n e^{-i\beta_n h}\left[\beta_n - Z_s\left(\frac{\omega}{c}\right)\right] - B_n e^{i\beta_n h}\left[\beta_n + Z_s\left(\frac{\omega}{c}\right)\right]\right)\right\}. \qquad (29)$$

Similarly integrating (20) and (22) over limits of validity after projecting over exponential vectors, we obtain

$$\tau_m\left[\eta_m + Z_s\left(\frac{\omega}{c}\right)\right]$$

$$= \sum_{n=0}^{\infty}\left\{\tilde{I}_{m,n}^-\left(A_n\left[\beta_n + Z_s\left(\frac{\omega}{c}\right)\right] - B_n\left[\beta_n - Z_s\left(\frac{\omega}{c}\right)\right]\right)\right\}. \qquad (30)$$

Substituting (30) in (24), (29) in (23) and rewriting as a system of equations,

$$\left\{\delta_{m,p} - \frac{2}{1+\delta_{m,0}}\left[\beta_p + Z_s\left(\frac{\omega}{c}\right)\right] \sum_{n=-\infty}^{\infty} \frac{I_{n,m}^+ \tilde{I}_{n,p}^-}{\eta_n + Z_s(\omega/c)}\right\} A_p$$

$$+ \left\{\delta_{m,p} + \frac{2}{1+\delta_{m,0}}\left[\beta_p - Z_s\left(\frac{\omega}{c}\right)\right]\right.$$

$$\left. \times \sum_{n=-\infty}^{\infty} \frac{I_{n,m}^+ \tilde{I}_{n,p}^-}{\eta_n + Z_s(\omega/c)}\right\} B_p = 0, \qquad (31)$$

$$e^{-i\beta_p h}\left\{\delta_{m,p} + \frac{2}{1+\delta_{m,0}}\left[\beta_p - Z_s\left(\frac{\omega}{c}\right)\right] \sum_{n=-\infty}^{\infty} \frac{I_{n,m}^+ \tilde{I}_{n,p}^-}{\eta_n + Z_s(\omega/c)}\right\} A_p$$

$$+ e^{i\beta_p h}\left\{\delta_{m,p} - \frac{2}{1+\delta_{m,0}}\left[\beta_p + Z_s\left(\frac{\omega}{c}\right)\right]\right.$$

$$\left. \times \sum_{n=-\infty}^{\infty} \frac{I_{n,m}^+ \tilde{I}_{n,p}^-}{\eta_n + Z_s(\omega/c)}\right\} B_p = I_{0,m}^+ \frac{2}{1+Z_s} \frac{2}{1+\delta_{m,0}}, \qquad (32)$$

(31) and (32) constitute a matrix system that can be solved for the mode amplitudes inside the slots, i.e. A_m and B_m. The boundary conditions can be used to find t and r, and these can be substituted back into the respective equations to find the electromagnetic field enhancements.

2.3. Drude model for permittivity

For polar materials like InSb, Drude model describes the frequency dependence of the relative permittivity,

$$\varepsilon(\omega) = \varepsilon(0) - \frac{\omega_{p0}^2}{\omega(\omega + j\tau^{-1})}, \qquad (33)$$

when the frequency is smaller than transverse optical phonon frequency. Here $\varepsilon(0)$ is the static dielectric constant and is 16.8 for InSb (11.7 for Si), τ is the relaxation time of the electrons, $\omega_{p0} = \omega_p \sqrt{\varepsilon(0)/\varepsilon_0}$, $\omega_p = \sqrt{N_d e^2/\varepsilon(0)m^*}$ is the plasma frequency, N_d is the charge carrier concentration, e is the electronic charge, and m^* is the electron effective mass. The mobility of the carriers is related to the relaxation time by

$$\mu = \frac{e\tau}{m^*}. \qquad (34)$$

For metals, relative permittivity

$$\varepsilon(\omega) = 1 - \frac{\omega_{p0}^2}{\omega(\omega + j\tau^{-1})}. \qquad (35)$$

3. Choice of parameters

The test frequency was chosen to be $14 \, \text{cm}^{-1}$, since absorption peaks of interest to FTIR transmission spectroscopy of biological molecules occur in this region. At room temperature $(300 \, \text{K})$, InSb has an electron mobility [27] of $7.7 \cdot 10^4 \, \text{cm}^2 \cdot \text{V}^{-1} \cdot \text{s}^{-1}$. The corresponding carrier concentration is $1.1 \cdot 10^{16} \, \text{cm}^{-3}$ (close to intrinsic). From equations InSb was found to have a relative permittivity of $-242.9 + i160.5$. The plasma frequency was $\sim 0.5 \, \text{THz}$. Si has an electron mobility of $950 \, \text{cm}^2 \cdot \text{V}^{-1} \cdot \text{s}^{-1}$ [28] and a corresponding carrier concentration of $10^{17} \, \text{cm}^{-3}$. The relative permittivity is $-9.5 + i57.3$ and the plasma frequency $0.48 \, \text{THz}$. For Au, relative permittivity is huge $-5.56 \cdot 10^4 + i1.22 \cdot 10^6$ and plasma frequency $2.17 \cdot 10^3 \, \text{THz}$ [29].

Since our region of interest in THz is $10-25 \, \text{cm}^{-1}$, we had to choose a spacing that was less than the smallest wavelength of the incident radiation i.e. $400 \, \mu\text{m}$. Modeling was conducted for two different periodicity values, $d = 381$ and $251 \, \mu\text{m}$. Due to the high absorbing part of InSb, Si permittivity and the limitation of the perfect conducting wall approximation for slots in Au, the thickness was chosen to be small $(h < 12 \, \mu\text{m})$.

In the case of the Fourier expansion method for InSb and Si, the discontinuous permittivity function of the modulated medium theoretically needs an infinite mode representation. However, convergence of transmission and the electromagnetic field enhancements was achieved after a finite Fourier sum of modes (764 for $d = 381 \, \mu\text{m}$ and 504 for $d = 251 \, \mu\text{m}$). The results were also checked for possible errors by considering only the real part of the permittivity function and running the model to satisfy energy conservation requirements $(|t|^2 + |r|^2 = 1)$. Convergence with just a dominant real permittivity is very difficult to achieve. In the analysis of the Au structure using the surface impedance boundary conditions method, just 8 modes inside the slit were more than enough to ensure convergence. 3000 transmitted (reflected) orders were considered.

4. Results and discussion

The far-field transmission of the InSb structure, $|t|$, was calculated as a function of frequency for the optimum slot width $s = 55 \, \mu\text{m}$ and two different periodicities, with $h = 4 \, \mu\text{m}$. The results at $d = 381 \, \mu\text{m}$ are plotted in Fig. 2. Since the permittivity of InSb is modulated periodically and changes substantially across $10-25 \, \text{cm}^{-1}$, we notice peaks in the transmission characteristics. At the high frequency end, the permittivity approaches closer to the behavior of metals (closer to the plasma frequency), at optical frequencies thereby leading to an increase in transmission. The low level of transmission in the InSb case is due to the predominantly metallic behavior of the structure in this frequency range. The overall transmission magnitude is higher for a s maller periodicity at the same s/d ratio,
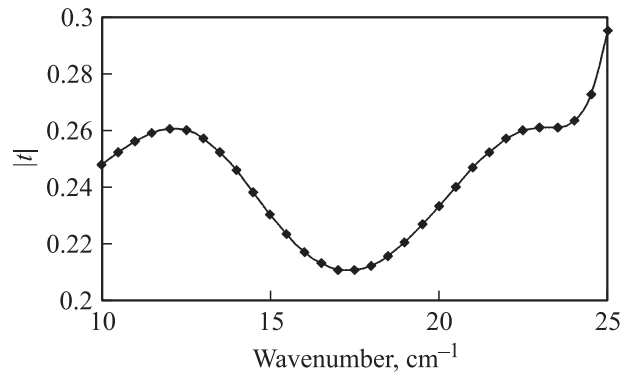
Figure 2. Transmittance, $|t|$, through InSb structure as a function of wavenumber. $d = 381 \, \mu\text{m}$, $s = 55 \, \mu\text{m}$ and $h = 4 \, \mu\text{m}$.
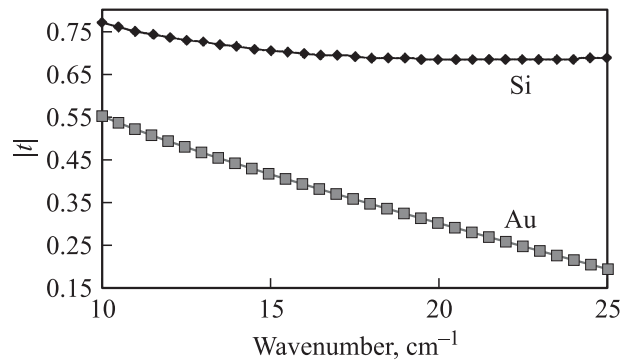
Figure 3. Transmittance, $|t|$, through Si and Au structures as a function of wavenumber for optimized parameters: $d = 251 \, \mu\text{m}$, $s = 95 \, \mu\text{m}$ for Si; $d = 251 \, \mu\text{m}$, $s = 36 \, \mu\text{m}$ for Au; $h = 4 \, \mu\text{m}$ in both cases.

thickness and frequency. This increase in transmission points to the effect of slot interactions since at $d = 251 \, \mu\text{m}$ the slots are closer to each other.

In the case of Si and Au, the change in permittivity throughout the frequency range of interest is very small. This is the reason for the absence of peaks in the transmission characteristics as shown in Fig. 3. Optimum parameters for Si $(d = 251 \, \mu\text{m}, \, s = 95 \, \mu\text{m})$ and Au $(d = 251 \, \mu\text{m}, \, s = 36 \, \mu\text{m})$ were used. The smaller absorbing component in Si (when compared to InSb) leads to larger transmission. Slots in Au offer large transmission owing to a dominant $m = 0$ mode. Our assumption of a small film thickness $(h \ll \lambda)$ forbids resonance peaks in the transmission characteristics in all cases.

The electric field amplitudes at the incident interface, $|E_x^i/E_0|$ (or $|E_x^i|$ in the Au case), were calculated as a function of the x-coordinate for the optimized structures. The strong electric field enhancement occurred within the sub-micrometer region around the slot edges i.e. at discontinuities. InSb offers the maximum enhancement as expected (the ratio of the magnitude of the real component of permittivity to absorbing component is highest). Fig. 4 shows the enhancement, $|E_x^i/E_0|$, as a function of x-coordinate for an InSb structure with $s = 55 \, \mu\text{m}$ and $h = 4 \, \mu\text{m}$,
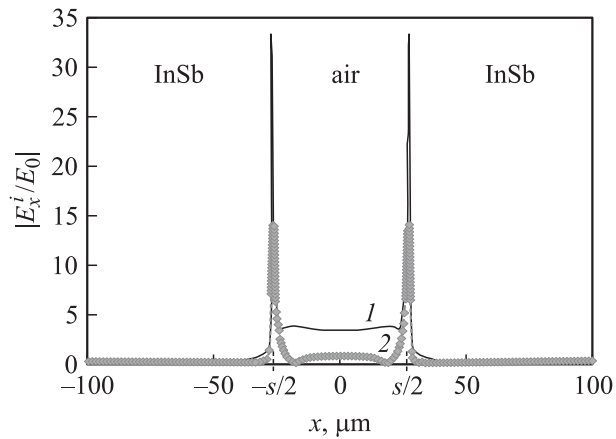
Figure 4. Electric field enhancement, $|E_x^i/E_0|$, as a function of x in InSb structure with $d = 381\,\mu$m, $s = 55\,\mu$m and $h = 4\,\mu$m, for $\lambda = 714$ (*1*) and $417\,\mu$m (*2*). Note, the majority of the enhancement takes place at the slot edges i.e. around $(-s/2)$ and $(s/2)$.
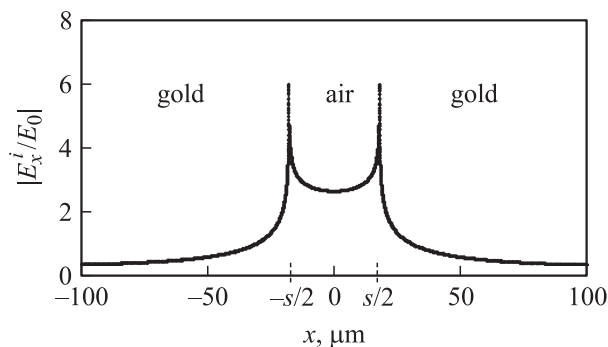

Figure 5. Electric field enhancement, $|E_x^i/E_0|$, as a function of x in gold structure with $d = 251\,\mu$m, $s = 36\,\mu$m and $h = 4\,\mu$m, for $\lambda = 714\,\mu$m.

for the radiation frequencies of 14 and $24\,\text{cm}^{-1}$. Practically most of the fields were confined to the edges i.e. sharp regions of the conducting medium. The enhancement at the edges was an order of magnitude higher than at other points within the slot. For the radiation frequency of $14\,\text{cm}^{-1}$, the maximum field enhancement was 33.3 at the incident interface and 31.8 at the outgoing interface for $h = 4\,\mu$m. For $h = 6\,\mu$m, these values were 27.7 and 25 respectively and for $h = 12\,\mu$m, 20.5 and 14.7 respectively. The half power width around the slot edges was $\sim 500\,$nm with maximum power enhancement ~ 1100 for the $h = 4\,\mu$m case. This region did not change much for the other h values and Si, Au structures. The enhancement also exists across the entire slot region, slightly decreasing in the z-direction from the incident interface to the outgoing interface. It is higher at the radiation frequency of $14\,\text{cm}^{-1}$ compared to $24\,\text{cm}^{-1}$. Si offered a maximum power enhancement of ~ 125 and Au ~ 31.5 for the same height, frequency $(14\,\text{cm}^{-1})$ and the respective optimized parameters $(d = 251\,\mu$m, $s = 95\,\mu$m for Si, $d = 251\,\mu$m,

$s = 36\,\mu$m for Au — see Fig. 5). These edge effects are due to evanescent fields and therefore decay very abruptly in the z-direction of the medium of incidence.

In addition to $|E_x^i/E_0|$, we calculated the distribution of the z-component of electric field, $|E_z^i/E_0|$, along the x-coordinate, and found that both components behave approximately in accordance with edge effects [30] in our low-frequency range. The z-component is negligibly small in the entire slot region except around the edges, which confirms the approximate TEM mode in the slot region. The enhancement mechanism cannot be attributed to a surface plasmon mode since the plasmon matching condition [6] is not appropriate for permittivities with substantial imaginary parts and for structures with small thickness $(h \ll \lambda)$.

5. Summary and conclusions

In this paper, we have modeled subwavelength array of rectangular slots in semiconductors (InSb, Si) and metals (Au), compared the results and demonstrated strong electric field edge effects in propagation of THz radiation through the periodic structure. The detailed theory for each method (Fourier expansion and surface impedance boundary conditions) was shown. InSb, owing to the highest ratio of real to imaginary components of its permittivity, offered the highest electromagnetic field enhancement at slot edges. Since the assumed thickness was small, non-anomalous behavior of far-field transmission was observed in all cases. The strongly enhanced local electromagnetic fields near slot edges can potentially be used for the development of novel bio-photonic sensors with the radiation to bio-material coupling enhancement factors on the order of 1000, leading to a substantial increase in detection sensitivity. Another possible application is in sensing changes of dielectric properties of biomaterials [31,32] in biophysical processes, for example, denaturation of DNA. Since Si and Au structures are easier to fabricate than InSb and offer reasonable enhancement factors themselves, the realization of a first principle novel biosensor is not far off.

Part of this work was published in [33].

References

[1] T. Globus, D. Woolard, M. Bykhovskaia, B. Gelmont, L. Werbos, A. Samuels. Int. J. of High Speed Electron. Syst., **13**, 903 (2003).

[2] T. Globus, D. Woolard, T.W. Crowe, T. Khromova, B. Gelmont, J. Hesler. J. Phys. D: Appl. Phys., **39**, 3405 (2006).

[3] A. Bykhovski, T. Globus, T. Khromova, B. Gelmont, D. Woolard. Proc. SPIE, **6212**, 62120H (2006).

[4] M.E. McDonald, A. Alexanian, R.A. York, Z. Popovic, E.N Grossman. IEEE Trans. On Microwave Theory and Techniques, **48**, 712 (2000).

[5] *Electromagnetic Theory of Gratings*, ed. by R. Petit (Springer-Verlag, Berlin Heidelberg, 1980).

[6] P. Sheng, R.S. Stepleman, P.N. Sanda. Phys. Rev. B, **26**, 2907 (1982).

[7] H.E. Went, A.P. Hibbins, J.R. Sambles, C.R. Lawrence, A.P. Crick. Appl. Phys. Lett., **77**, 2789 (2000).

[8] Q. Cao, P. Lalanne. Phys. Rev. Lett., **88**, 057 403 (2002).

[9] T.W. Ebbesen, H.J. Lezec, H.F. Ghaemi, T. Thio, P.A. Wolff. Nature, **391**, 667 (1998).

[10] H.F. Ghaemi, T. Thio, D.E. Grupp, T.W. Ebbesen, H.J. Lezec. Phys. Rev. B, **58**, 6779 (1998).

[11] T. Thio, H.F. Ghaemi, H.J. Lezec, P.A. Wolff, T.W. Ebbesen. J. Opt. Soc. Amer. B, **16**, 1743 (1999).

[12] E. Popov, M. Neviere, S. Enoch, R. Reinisch. Phys. Rev. B, **62**, 16 100 (2000).

[13] L. Martin-Moreno, F.J. Garcia-Vidal, H.J. Lezec, K.M. Pellerin, T. Thio, J.B. Pendry, T.W. Ebbesen. Phys. Rev. Lett., **86**, 1114 (2001).

[14] S.A. Darmanyan, A.V. Zayats. Phys. Rev. B, **67**, 035 424 (2003).

[15] S.H. Chang, S.K. Gray. Opt. Express, **13**, 3150 (2005).

[16] H. Cao, A. Nahata. Opt. Express, **12**, 1004 (2004).

[17] D. Qu, D. Grischkowsky, W. Zhang. Opt. Lett., **29**, 896 (2004).

[18] J. Gomez Rivas, C. Schotsch, P. Haring Bolivar, H. Kurz. Phys. Rev. B, **68**, 201 306(R) (2003).

[19] J. Gomez Rivas, C. Janke, P. Haring Bolivar, H. Kurz. Opt. Express, **13**, 847 (2005).

[20] H. Raether. *Surface Plasmons on Smooth and Rough Surfaces and on Gratings* (Springer-Verlag, Berlin, 1988) [Springer Tracts in Modern Physics, vol. **111**, ch. 2,4,5].

[21] E. Popov, S. Enoch, G. Tayeb, M. Neviere, B. Gralak, N. Bonod. Appl. Opt., **43**, 999 (2004).

[22] J.W. Lee, M.A. Seo, D.J. Park, S.C. Jeoung, Q.H. Park, Ch. Lienau, D.S. Kim. Opt. Express, **14**, 12 638 (2006).

[23] J.A. Porto, F.J. Garcia-Vidal, J.B. Pendry. Phys. Rev. Lett., **83**, 2845 (1999).

[24] F.J. Garcia-Vidal, L. Martin-Moreno. Phys. Rev. B, **66**, 155 412 (2002).

[25] G.B. Arfken, H.J. Weber. *Mathematical Methods for Physicists*, 4th ed. (Academic Press, 1995) ch. 14, p. 836.

[26] A. Wirgin, T. Lopez-Rios. Opt. Commun., **48**, 416 (1984).

[27] E. Litwin-Staszewska, W. Szymanska, P. Piotrzkowski. Phys. Status Solidi B, **106**, 551 (1981).

[28] S.S. Li, W.R. Thurber. Sol. St. Electron, **20**, 609 (1977).

[29] A. Heltzel, S. Theppakuttai, S.C. Chen, J.R. Howell. Nanotechnology, **19**, 025 305 (2008).

[30] J.D. Jackson. *Classical Electrodynamics*, 2nd ed. (John Wiley & Sons Inc., 1975) ch. 2, p. 77.

[31] R. Parthasarathy, T. Globus, T. Khromova, N. Swami, D. Woolard. Appl. Phys. Lett., **87**, 113 901 (2005).

[32] N.S. Swami, C.F. Chou, R. Terberueggen. Langmuir, **21**, 1937 (2005).

[33] R. Parthasarathy, A. Bykhovski, B. Gelmont, T. Globus, N. Swami, D. Woolard. Phys. Rev. Lett., **98**, 153 906 (2007).

Редактор Л.В. Шаронова